Paleo-ENSO influence on African environments and early modern humans

Stefanie Kaboth-Bahr[1,2*], William D. Gosling[3], Ralf Vogelsang[4], André Bahr[2], Eleanor M. L. Scerri[4,5,6], Asfawossen Asrat[7], Andrew S. Cohen[8], Walter Düsing[1], Verena E. Foerster[9], Henry F. Lamb[10,11], Mark A. Maslin[12,13], Helen M. Roberts[10], Frank Schäbitz[9], Martin H. Trauth[1]

[1] University of Potsdam, Institute of Geosciences, Potsdam, Germany

[2] University Heidelberg, Institute of Earth Sciences, Heidelberg, Germany

[3] University of Amsterdam, Institute for Biodiversity and Ecosystem Dynamics, Amsterdam, Netherlands

[4] University of Cologne, Department of Prehistoric Archaeology, Cologne, Germany

[5] Pan-African Evolution Research Group, Max Planck Institute for the Science in Human History, Jena, Germany

[6] Department of Classics and Archaeology, University of Malta, Msida, Malta

[7] Addis Ababa University, School of Earth Sciences, Addis Ababa, Ethiopia

[8] University of Arizona, Department of Geosciences, Tucson, USA

[9] University of Cologne, Institute of Geography Education, Cologne, Germany

[10] Aberystwyth University, Department of Geography and Earth Sciences, Aberystwyth, UK

[11] University of Dublin, Trinity College, Department of Botany, Dublin, Ireland

[12] University College London, Department of Geography, London, UK

[13] Natural History Museum of Denmark, University of Copenhagen, Copenhagen, Denmark

Email: Stefanie Kaboth-Bahr; kabothbahr@uni-potsdam.de

Classification

Earth, Atmospheric, and Planetary Sciences and/or Environmental Sciences and Ecology and/or Anthropology and/or Human environmental Sciences.

Keywords

African paleoclimate, hominin evolution, Walker and Hadley Circulation, orbital forcing

Author Contributions

SKB, WDG, RV and AB conceived and designed the study with contributions from EMLS, AA, ASC, WD, VF, HFL, MM, HMR, FS and MHT. SKB, AB, WDG, WD, VF and MHT compiled, processed and analysed the data. SKB wrote the manuscript with contributions from all authors and prepared

the figures. All authors read and refined the manuscript. All authors have approved the submitted version of this manuscript.

This PDF file includes:

Main Text
Figures 1 to 3
Materials and Methods

Abstract

In this study we synthesize terrestrial and marine proxy records spanning the last 620 thousand years, to decipher pan-African climate variability, its drivers and potential linkages to hominin evolution. We find a tight correlation between moisture availability across Africa to Walker and Hadley Circulation variability that was most likely driven by changes in Earth's eccentricity. Our results demonstrate that low latitude insolation was a prominent driver of pan-African climate change during the mid to late Pleistocene. We argue that these low-latitude climate processes governed the dispersion and evolution of vegetation, as well as mammals, in eastern and western Africa, by increasing resource-rich and stable ecotonal settings thought to have been important to early modern humans.

Significance Statement

Our results identify the prime driver of climate variation in Africa's low latitudes over the last 620 thousand years – the key timeframe for the evolution of our species. Warming and cooling of the tropical Pacific Ocean paced by insolation changes modulated the tropical Walker Circulation, driving opposing wet-dry states in eastern and western African. We show that the effects of glacial/interglacial cycles were not the predominant source of environmental change in most of the continent. Africa's environmental patchwork driven by low latitude climate processes should therefore be a critical component in conceptual models of human evolution and early demography over the past 620 thousand years.

Introduction

The role of climatically driven environmental change in triggering key stages of hominin evolution over the last 6 million years has long been recognised (1–3). More recently, environmental changes across Africa have been implicated in major shifts in the population structure of hominins over the last half a million years – the key demographic context for the emergence of *Homo sapiens* (4–8). However, evaluating the impact of environmental changes and their possible effects on hominin evolution and demography is difficult, as high resolution climate archives are temporally and spatially sparse (9–11). Further problems are introduced by the fact that available proxy studies usually detail climate variability of only one study site or region (3, 12, 13), which makes it difficult to study its consequences for evolutionary processes across large spatial scales. Here, we provide the first pan-African view on climate change during the mid to late Pleistocene, in order to construct a framework for understanding hominin evolution within this time frame. To achieve this, we have combined eleven terrestrial lacustrine and marine sedimentary archives (Fig. 1; Table S1, S2; see details on site selection criteria in the supplementary information) detailing wet-dry variability of eastern and western Africa during the last 620 thousand years (kyr) – the time interval of the emergence of *Homo sapiens* in Africa and its subsequent out-of-Africa dispersal (see Fig. 1, Tab. S1).

Today the climate of tropical Africa is governed by convection with the seasonal migration of the tropical rainbelt dictating the pattern of precipitation (9). Changes in seasonal positioning of the rainbelt relate to insolation variability with rainfall occurring in northern/southern Africa during boreal/austral summer (14). In addition, observational data suggest that African climate is highly sensitive to changes in the Walker Circulation (WC), which is manifested via the El Niño Southern Oscillation (ENSO) (15, 16; see Supplementary Information for more details). ENSO originates from sea-surface temperature anomalies in the equatorial Pacific Ocean, and these changes impact the atmospheric WC, which in turn alters the location and strength of tropical convection cells (Fig. 1) (17). Through this coupled ocean-atmosphere system, ENSO events are propagated around the globe by Kelvin and Rossby waves (16) eventually reaching the African continent (see Supplementary Information for more details). Here, changes in ENSO state alter the east-west trending moisture gradient across Africa (18–20). This leads to opposing dry and humid conditions between eastern and western Africa, so that during La Niña eastern Africa experiences drier conditions than western Africa and vice versa during El Niño events. For instance, during El Niño years eastern Africa experiences positive precipitation anomalies of up to 60% (or 200 mm per year) relative to the yearly precipitation budget during non-El Niño years, whilst western Africa experiences a 20-40% precipitation reduction (21, 22). Besides these modern driving mechanisms, spatiotemporal precipitation changes in Africa on much longer time scales have also been attributed to changes in Atlantic Meridional Overturning Circulation, global atmospheric CO_2 concentrations (pCO_2), and/or the waning and waxing of global ice sheets (23–26). However, the interplay of these various driving mechanisms on orbital time scales and their pan-African impact on precipitation remains ambiguous.

Results

Our study elucidates the spatiotemporal variability of the African hydroclimate and its driving forces by providing a comprehensive analysis of pan-African climate change during the last ~620 kyr. To parametrize pan-African climate variability we performed a piecewise principal component analysis (pwPCA; see methods for details) of the selected data sets (see Fig. 1 and 2) to account for differences in temporal length of the records. The resulting first principal component (PC1), capturing the maximum variance of the data, accounts on average for 30% of the variance observed in all the data sets and clearly depicts an east-west dipole of the studied sites (Fig. 2B). Remaining principle components (PCs) account individually for less than 10% of the remaining data variance. This suggests that the observed east-west dipole is the predominant mode of signal variability on a pan-African scale during the last ~620 kyr. In detail, the eastern African sites (CHB, MED, MAG and LOM; reflecting the negative PC1 branch; Fig. 1) oppose western African sites

(SAH, BOS, LIB, CON, NAM1 and NAM2; the positive PC1 branch; Fig. 1). MAL located in southeastern Africa is weakly in phase with the western African sites (Note: here the applied age model for MAL is one of several possibilities. Please see SI for the PC1 comparison based on different MAL age models).

The reconstructed pan-African climate variability, represented by PC1, clearly depicts four phases during the last ~620 kyr that have been constrained by break point analysis (Fig. 2C; see methods for details). Phase I lasts from ~620 kyr to roughly ~525 kyr and is characterized by more humid conditions in eastern Africa and more arid conditions in western Africa (i.e. PC1 shows more negative values). This pattern reverses during subsequent Phase II between ~525 kyr and ~279 kyr, when above average humid conditions prevail in western Africa, while eastern Africa experiences more arid conditions (i.e. PC1 shows more positive values). Notably, Phase II encompasses two sub-phases with a transition at around ~400 kyr. However, the median over the entire variability of Phase II is significantly more positive in its PCA loadings than Phases I and III. Based on this difference we decided to group both sub-phases into Phase II. During Phase III between ~279 kyr and ~128 kyr this relationship once again reverses with pronounced humid conditions prevailing in eastern Africa and arid conditions in western Africa. Late Phase III aligns, within the limitation of the age uncertainties, with the well documented wet phase associated with the last interglacial (~129–119 kyr) (12). During the last ~128 kyr (Phase IV) more humid conditions prevailed in western Africa in contrast to a drier eastern Africa.

Discussion

In order to decipher the mechanism behind the observed pan-African moisture pattern, we first considered low latitude insolation changes as a strong contributor, given the well-documented sensitivity of tropical climate to insolation changes (27). Thus, we first compared the PC1 to precession and orbital eccentricity variability for the studied time interval (Fig. 2A). PC1 clearly follows the distinctive ~400 kyr and ~100 kyr beats of eccentricity, which is further supported by the near synchronicity of the break points calculated from PC1 and orbital eccentricity forcing (Fig. 2). This coherent pattern suggests that on geological time scales precipitation changes in tropical Africa are in large parts paced by insolation changes (28). However, by itself, eccentricity only has a small net effect on the annual mean insolation (<0.5%). Instead it exerts a strong pull on the amplitude change of orbital precession (29). The difference in precession amplitude can amount to ~10% of the annual mean insolation (20). Changes in the annual insolation budget and thus increased/decreased regional convection above the African continent could potentially explain the difference between northern and southern Africa, as it does today on seasonal timescales. However, it does not fully explain the east-west moisture dipole apparent in PC1. To explain this conundrum, we thus require an insolation-sensitive mechanism that generates zonal changes in precipitation. We hypothesize that ENSO-like variability might be the key to unravel this enigma. It has been demonstrated that ENSO modulated Earth's climate during the geological past (28, 29). Also, it has been shown that ENSO variability is sensitive to insolation changes (17) with high eccentricity/low eccentricity (increased/decreased insolation) aligning with El Niño-like/La Niña-like conditions (30). Finally, modern ENSO-related modifications in the WC (31) result in a westward/eastward shift of convection over Africa (15, 18).

To ground-truth the potential role of ENSO-like fluctuations for generating the observed zonal precipitation gradients, we compared PC1 to the east-west sea-surface temperatures (SST) gradient of the Pacific Ocean ($\Delta SST_{806\text{-}846}$; Fig. 2D) during the last ~620 kyr (32, 33). A strong positive ΔSST indicates a warmer west Pacific relative to a colder east Pacific Ocean, similar to modern La Niña conditions. On the other hand, a strongly reduced $\Delta SST_{806\text{-}846}$ suggests a warming in the east Pacific Ocean, and thus resembles modern El Niño conditions (30). The comparison shows a strong resemblance between PC1 and $\Delta SST_{806\text{-}846}$ throughout the last ~620 kyr which is further supported by similar timed break points in both records (Fig. 2). This implies that the dominant climate signal follows a paleo-ENSO beat, with contrasting effects in eastern and western Africa. This suggests that traces of the hypothesized WC shifts induced by ENSO variability during the last ~620 kyr should also be preserved in proxy records from the Atlantic and Indian Ocean.

Indeed, the analysis of the SST variability of Arabian Sea ODP Site 722 clearly depicts a strong warming during the proposed El Niño-like condition of Phase III (33) in line with our expectation (Fig. S2). The simultaneous formation of the Atlantic cold tongue as previously proposed is also visible in the SST cooling during Phase III of tropical Atlantic Ocean site V30-40 (34). This provides further strong indication of the sensitivity of the pan-African moisture budget to changes in the WC during the last ~620 kyr (Fig. S2).

The results we present here provide a new framework for understanding E-W contrasts in Africa's climatic history on geological time scales, which has important implications for testing hypotheses regarding human evolution and the dispersal of early modern humans. For this we have outlined the spatiotemporal effects of ENSO-like variability during Phases II to IV, comprising a full ~400 kyr eccentricity cycle in Figure 3. We find that during eccentricity minima and ensuing La Niña-like conditions (i.e. Phases II and IV) regions of low topographic complexity (35) from the Sahel to Namibia were preconditioned to wetter conditions (Fig. 3D and F). In contrast, eccentricity maxima and thus El Niño-like conditions (i.e. Phase III) favored a moisture increase across the topographically more complex and geographically smaller eastern Africa (Fig. 3E) (35). Although our analysis does not allow for the quantification of the observed relative humidity changes, these paleoclimatic changes and their effects on terrestrial ecosystems are likely to have impacted human dispersal and evolution. While the association between climate and the human record is typically neither simple nor direct, key linkages can be identified through proxy archives of vegetation changes as well as the mammalian record (36). In fact, our inferred paleo-ENSO driven humidity changes coincide with major changes in vegetation across the African continent during the last ~500 kyr. At the available terrestrial, landscape scale (i.e. 10s kms), pollen-based reconstructions of past-vegetation change at Lake Bosumtwi (western Africa) during the last ~500 kyr indicate oscillations between open forest and wooded savanna during La Niña-like conditions (Phase IV and II) and treeless savanna coinciding with El Niño-like conditions (Phase III) (37). The reverse is true for Lake Magadi (eastern Africa) where abundant Afromontane and woodland elements dominate during the El Niño phase (Phase III) and an the expansion of savanna during the La Niña phases (Phase II and IV) (3). Additionally, marine pollen records, which integrate a vegetation signal from a wide geographic area (100s kms), suggest a major perturbation on a pan-African scale at around ~128 kyr (38).

The impact of the inferred paleo-ENSO induced reorganization of the African climate system and associated changes in vegetation likely also had a profound ecological impact on mammal species across Africa. While the genetic diversity of many mammals is known to strongly reflect ecoregion biogeographic history and fragmentation, the driving factors for these community-wide patterns of vicariance are usually assumed to relate to environmental changes driven by climatic variability (39, 40). Interestingly, basal divisions during the Mid to Late Pleistocene between taxa repeatedly followed an oblique divide between western-central African populations and eastern-southern African populations that corresponds well with the rainfall dipole in our conceptual model (39–43). In addition, several studies attempting to constrain the timing of divergence in African mammals suggest that splits are out of phase with glacial-interglacial cycles, and instead linked population isolation and habitat fragmentation with pronounced, insolation driven oscillations between wet and dry conditions (41, 42). These time estimates for divergence correspond well with our proposed climatic phases. For example, the transition between Phase II and III, which saw the shift from wet to arid conditions in western-central Africa, dovetails with a general radiation of giraffe (*Cervus camelopardalis*), lion (*Panthera leo*), and hartebeest (*Alcelaphus buselaphus*), particularly with estimated split times between west/north and east/south clades (41, 42, 44). Additionally, the transition from Phase III to IV, which featured the return of wet/dry conditions in western-central/eastern-southern Africa corresponds with successive branching and population increase among giraffe, lion, and hartebeest in both regions (41, 42, 44). Many other taxa exhibit similar patterns, including African buffalo (*Syncerus caffer*), roan (*Hippotragus equinus*), waterbuck (*Kobus ellipsiprymnus*), kob (*Kobus kob*), warthog (*Phacochoerus africanus*), topi (*Damaliscus lunatus jimela*), and bushbuck (*Tragelaphus scriptus*) (40, 41, 43, 45). Specifically, phylogenetic patterns indicate the presence of refugial zones for savannah and grassland species in western Africa, southern Africa and a refugial mosaic/suture zone in eastern Africa. These areas likely

played a key role in fragmenting savannah and grassland species during the alternating periods of forest expansion associated with wetter conditions in western-central Africa or eastern Africa (42, 43, 46–48).

Although no ancient African DNA from these timeframes is available for humans, it seems likely that hominin populations have followed a similar pattern. Our findings are in fact consistent with previous studies that have indicated that archaeological site abundances in eastern Africa and elsewhere in tropical Africa are both inversely related up to 60 ka, and do not strongly align with glacial-interglacial cycles (49). Increases in abundance seem to correlate with periods of decreased humidity, for example between ~115-90 ka in tropical Africa, while decreases seem to correlate with increased humidity, for example between ~110-95 ka in eastern Africa, both of which fall within our Phase IV (49). The effects of the reconstructed paleo-ENSO variability likely caused forest fragmentation in eastern and western Africa during dry phases, which would have increased the size of ecotonal regions, that have long been argued to represent resource-rich, and therefore preferred habitats for hominins (49–51). Ecotonal areas may have provided important zones of habitat stability and population growth during the identified phases (Fig. 3), and critically, are also linked to the success of other African generalist mammals (40). These spatial patterns may explain past population structures reflecting deep regional sub-divisions that are likely to have been even more pronounced in the mid and late Pleistocene (7, 8, 48, 52–54).

Conclusion

Our results highlight a tight correlation between moisture availability in Africa and WC changes most likely induced by paleo-ENSO variability. This process causes a distinct east-west dipole with humid condition on one side of Africa and arid conditions on the other. We argue that the pacing of this low latitude process governed the dispersion and evolution of vegetation as well as mammals in eastern and western Africa, and likely also drove shifts in the degree of structure, population density, and core habitation areas of hominins. These results therefore provide a new framework to test a range of conceptual models regarding the multi-regional rise and subsequent dispersal of hominins (8) in which glacial-interglacial cyclicity can no longer be uncritically invoked as the predominant climatic driver.

Materials and Methods

Piecewise PCA (pwPCA)

Principal component analysis (PCA) detects linear dependencies between variables and replaces groups of linear correlated variables with new, uncorrelated variables referred to as the “principal components” (PCs). Since the first principal component (PC1) contains the highest variance, the PC2 the second highest variance, the last PCs are ignored to generally ignored to reduce the dimensions of the data. The principal component loadings (i.e. the coefficients of the linear combination of the initial variables from which the principal components are constructed) can be used to interprete the PCs and hence to identify (or display) dominant variability patterns in time series. Prior to the application of the pwPCA all data sets were resampled at 1 kyr resolution. All data was standardized to unit variance using their individual mean and standard deviation. Prior to standardization we also log-transformed the data sets of CHB, LOM, SAH, BOS, LIB, CON, NAM1, and NAM2 (see Table S1 for acronyms) to account for outlier induced data skewing, and thus more closely approximate a normal distribution for these data sets. For the pwPCA, the entire data set was separated into three time frames fitting to the individual shortest data set of each time frame (see Fig. 2). This leads to a decrease of data sets and thus an increase of uncertainties with increasing time. PCA was conducted using the built-in function *princomp* in R (55). Loadings and explained variance of the PC1 was averaged over all time steps of the piecewise PCA.

Break point analysis

The break points derive from a fitting of a linear regression model to the data set as implemented in the *strucchange* package in R (56). The algorithm tests deviations from stability in a classical linear regression model with a pre-set of maximum *m*=5 breakpoints. The integrated optimization algorithm provides the optimized location of the break points as well as their 2.5% and 97.5% confidence intervals.

Median calculation

To analyse long-term changes in the moisture of each individual site we calculated the median over the full length of the respective data set as a cut-off value between humid and arid conditions. Subsequently, we calculated the median for Phase II–IV only, following the age designation of PC1 as stated in the main text, and compared it to the overall cut-off value. Following the individual interpretation of the proxy records (see Table S1) we assigned each phase to overall humid or arid conditions. For MED and BOS cut-off values of 0 and 57 were already defined in the respective publication (57, 58).

Acknowledgments

SKB received funding from an Open-Topic Postdoc fellowship of the University of Potsdam and acknowledges funding from the DFG through grant KA 4757/3-1. Support for Chew Bahir drilling was provided by Deutsche Forschungsgemeinschaft (DFG) through the Priority Program SPP 1006 ICDP as well as National Science Foundation (NSF) grant NSF-EAR1338553 to ASC. FS acknowledges further funding from the DFG through grants SCHA 472/13 and SCHA 472/18. MHT acknowledges funding from the DFG through grants TR 419/8, TR 419/10, and TR 419/16. In addition, FS acknowledges funding from the CRC 806 Research Project "Our way to Europe" - Project Number 57444011. HFL and HMR were funded by grant NE/K014560/1 from the UK Natural Environment Research Council. This is publication #No. to be added after paper acceptance# of the Hominin Sites and Paleolakes Drilling Project.

All data used in the analysis are available through their respective references. The results of the piecewise PCA (pwPCA) and break point analysis conducted in this study are appended to this submission.

References

1. J. Galway-Witham, J. Cole, C. Stringer, Aspects of human physical and behavioural evolution during the last 1 million years. *J. Quat. Sci*. **34**, 355–378 (2019).
2. N. E. Levin, Environment and Climate of Early Human Evolution. *Annu. Rev. Earth Planet. Sci.* **43**, 405–429 (2015).
3. R. B. Owen, *et al*., Progressive aridification in East Africa over the last half million years and implications for human evolution. *Proc. Natl. Acad. Sci. U. S. A.* **115**, 11174–11179 (2018).
4. C. M. Schlebusch, *et al*., Genomic variation in seven Khoe-San groups reveals adaptation and complex African history. *Science* **338**, 374–379 (2012).
5. C. M. Schlebusch, *et al*., Southern African ancient genomes estimate modern human divergence to 350,000 to 260,000 years ago. *Science* **358**, 652–655 (2017).
6. M. Lipson, *et al.*, Ancient West African foragers in the context of African population history. *Nature* **577**, 665–670 (2020).
7. E. M. L. Scerri, *et al.*, Did Our Species Evolve in Subdivided Populations across Africa, and Why Does It Matter? *Trends Ecol. Evo*l. **33**, 582–594 (2018).
8. E. M. L. Scerri, L. Chikhi, M. G. Thomas, Beyond multiregional and simple out-of-Africa models of human evolution. *Nat. Ecol. Evol*. **3**, 1370–1372 (2019).
9. R. Potts, Evolution and climate variability. *Science* **273**, 922–923 (1996).
10. P. Roberts, B. A. Stewart, Defining the 'generalist specialist' niche for Pleistocene Homo sapiens. *Nat. Hum. Behav*. **2**, 542–550 (2018).

11. A. Mounier, M. Mirazón Lahr, Deciphering African late middle Pleistocene hominin diversity and the origin of our species. *Nat. Commun.* **10**, 1–13 (2019).
12. H. F. Lamb, *et al.*, 150,000-year palaeoclimate record from northern Ethiopia supports early, multiple dispersals of modern humans from Africa. *Sci. Rep*. **8**, 1–7 (2018).
13. S. J. Ivory, *et al.*, Environmental change explains cichlid adaptive radiation at Lake Malawi over the past 1.2 million years. *Proc. Natl. Acad. Sci. U. S. A.* **113**, 11895–11900 (2016).
14. S. E. Nicholson, Climate and climatic variability of rainfall over eastern Africa. *Rev. Geophys.* **55**, 590–635 (2017).
15. S. E. Nicholson, J. C. Selato, The influence of La Nina on African rainfall. *Int. J. Climatol*. **20**, 1761–1776 (2000).
16. F. S. R. Pausata, *et al*., Greening of the Sahara suppressed ENSO activity during the mid-Holocene. *Nat. Commun*. **8**, 1–12 (2017).
17. P. J. Webster, "The large-scale structure of the tropical atmosphere" in General Circulation of the Atmosphere, J. Hoskins, R. P. Pearce, Eds. (1983), pp. 35–275.
18. C. P. de Oliveira, *et al*., The Influence of the Regional Hadley and Walker Circulations on Precipitation Patterns over Africa in El Niño, La Niña, and Neutral Years. *Pure Appl. Geophys*. **175**, 2293–2306 (2018).
19. N. H. Saji, *et al*., A dipole mode in the tropical Indian ocean. *Nature* **401**, 360–363 (1999).
20. D. J. Nash, *et al*., African hydroclimatic variability during the last 2000 years. *Quat. Sci. Rev.* **154**, 1–22 (2016).
21. I. Fer, *et al*., The influence of El Niño-Southern Oscillation regimes on eastern African vegetation and its future implications under the RCP8.5 warming scenario. *Biogeosciences* **14**, 4355–4374 (2017).
22. S. M. Moore, *et al*., El Niño and the shifting geography of cholera in Africa. *Proc. Natl. Acad. Sci. U. S. A.* **114**, 4436–4441 (2017).
23. J. E. Kutzbach, F. A. Street-Perrott, Milankovitch forcing of fluctuations in the level of tropical lakes from 18 to 0 kyr BP. *Nature* **317**, 130–134 (1985).
24. M. H. Trauth, *et al.*, Late Cenozoic moisture history of east Africa. *Science* **309**, 2051–2053 (2005).
25. I. S. Castañeda, *et al.*, Wet phases in the Sahara/Sahel region and human migration patterns in North Africa. *Proc. Natl. Acad. Sci. U. S. A*. **106**, 20159–20163 (2009).
26. P. N. DiNezio, *et al.*, Glacial changes in tropical climate amplified by the Indian Ocean. *Sci. Adv.* **4**, eaat9658 (2018).
27. A. C. Clement, R. Seager, M. A. Cane, Orbital controls on the El Nino/Southern Oscillation and the tropical climate. *Paleoceanography* **14**, 441–456 (1999).
28. A. Davies, *et al*., El Niño-Southern oscillation variability from the late cretaceous marca shale of california. Geology 40, 15–18 (2012).
29. T. Laepple, G. Lohmann, Seasonal cycle as template for climate variability on astronomical timescales. *Paleoceanography* **24** (2009).
30. Y. G. Zhang, *et al*., High resolution hematite and goethite records from ODP 1143, South China Sea: Co-evolution of monsoonal precipitation and El Niño over the past 600,000 years. *Earth Planet. Sci. Lett*. **264**, 136–150 (2007).
31. M. L. L'Heureux, S. Lee, B. Lyon, Recent multidecadal strengthening of the Walker circulation across the tropical Pacific. *Nat. Clim. Chang*. **3**, 571–576 (2013).
32. M. Medina-Elizalde, D. W. Lea, The Mid-Pleistocene transition in the tropical Pacific. *Science* **310**, 1009–1012 (2005).
33. T. D. Herbert, *et al.*, Late Miocene global cooling and the rise of modern ecosystems. *Nat. Geosci.* **9**, 843–847 (2016).
34. A. McIntyre, *et al.*, Surface water response of the equatorial Atlantic Ocean to orbital forcing. *Paleoceanography* **4**, 19–55 (1989).
35. G. N. Bailey, G. C. P. King, Dynamic landscapes and human dispersal patterns: Tectonics, coastlines, and the reconstruction of human habitats. *Quat. Sci. Rev*. **30**, 1533–1553 (2011).
36. A. K. Behrensmeyer, Climate change and human evolution. *Science* **311**, 476–478 (2006).

37. C. S. Miller, W. D. Gosling, Quaternary forest associations in lowland tropical West Africa. *Quat. Sci. Rev*. **84**, 7–25 (2014).
38. L. Dupont, Orbital scale vegetation change in Africa. *Quat. Sci. Rev*. **30**, 3589–3602 (2011).
39. M. de Manuel, et al., The evolutionary history of extinct and living lions. *Proc. Natl. Acad. Sci. U. S. A.* **117**, 10927–10934 (2020).
40. Y. Moodley, M. W. Bruford, Molecular biogeography: Towards an integrated framework for conserving Pan-African biodiversity. *PLoS One* **2**, e454 (2007).
41. D. M. Brown, et al., Extensive population genetic structure in the giraffe. *BMC Biol*. **5**, 57 (2007).
42. L. D. Bertola, et al., Phylogeographic Patterns in Africa and High Resolution Delineation of Genetic Clades in the Lion (Panthera leo). *Sci. Rep*. **6**, 30807 (2016).
43. E. D. Lorenzen, R. Heller, H. R. Siegismund, Comparative phylogeography of African savannah ungulates. *Mol. Ecol*. **21**, 3656–3670 (2012).
44. Flagstad, P. O. Syvertsen, N. C. Stenseth, K. S. Jakobsen, Environmental change and rates of evolution: The phylogeographic pattern within the hartebeest complex as related to climatic variation. *Proc. R. Soc. B Biol. Sci*. **268**, 667–677 (2001).
45. R. Barnett, N. Yamaguchi, I. Barnes, A. Cooper, The origin, current diversity and future conservation of the modern lion (Panthera leo). *Proc. R. Soc. B Biol. Sci*. **273**, 2119–2125 (2006).
46. G. Hewitt, The genetic legacy of the quaternary ice ages. *Nature* **405**, 907–913 (2000).
47. J. T. Faith, J. Rowan, K. O'Brien, N. Blegen, D. J. Peppe, Late Pleistocene Mammals from Kibogo, Kenya: Systematic Paleontology, Paleoenvironments, and Non-Analog Associations. *J. Vertebr. Paleontol*. **40**, e1841781 (2020).
48. J. T. Faith, et al., Paleoenvironmental context of the Middle Stone Age record from Karungu, Lake Victoria Basin, Kenya, and its implications for human and faunal dispersals in East Africa. *J. Hum. Evol*. **83**, 28–45 (2015).
49. M. W. Blome, A. S. Cohen, C. A. Tryon, A. S. Brooks, J. Russell, The environmental context for the origins of modern human diversity: A synthesis of regional variability in African climate 150,000-30,000 years ago. *J. Hum. Evol*. **62**, 563–592 (2012).
50. L. S. Basell, Middle Stone Age (MSA) site distributions in eastern Africa and their relationship to Quaternary environmental change, refugia and the evolution of Homo sapiens. *Quat. Sci. Rev*. **27**, 2484–2498 (2008).
51. C. Shipton, et al., 78,000-year-old record of Middle and Later stone age innovation in an East African tropical forest. *Nat. Commun.* **9**, 1–8 (2018).
52. A. Bergström, et al., Insights into human genetic variation and population history from 929 diverse genomes. *Science* **367**, eaay5012 (2020).
53. E. M. L. Scerri, et al., Continuity of the Middle Stone Age into the Holocene. *Sci. Rep*. **11**, 70 (2021).
54. A. Bergström, C. Stringer, M. Hajdinjak, E. M. L. Scerri, P. Skoglund, Origins of modern human ancestry. *Nature* **590**, 229–237 (2021).
55. W. N. Venables, B. D. Ripley, Modern Applied Statistics with S Fourth edition by (2002).
56. A. Zeileis, C. Kleiber, K. Walter, K. Hornik, Testing and dating of structural changes in practice. Comput. *Stat. Data Anal*. **44**, 109–123 (2003).
57. K. M. Grant, et al., A 3 million year index for North African humidity/aridity and the implication of potential pan-African Humid periods. *Quat. Sci. Rev*. **171**, 100–118 (2017).
58. C. S. Miller, W. D. Gosling, D. B. Kemp, A. L. Coe, I. Gilmour, Drivers of ecosystem and climate change in tropical West Africa over the past ~540 000 years. *J. Quat. Sci.* **31**, 671–677 (2016).
59. J. Laskar, et al., A long-term numerical solution for the insolation quantities of the Earth. *Astron. Astrophys*. **428**, 261–285 (2004).
60. I. McDougall, F. H. Brown, J. G. Fleagle, Stratigraphic placement and age of modern humans from Kibish, Ethiopia. *Nature* **433**, 733–736 (2005).

Figure 1. Suite of study sites and the global Walker Circulation (WC). (**A**) Location map of marine and terrestrial proxy records used for the reconstruction of African climate. Note the black dots associated with marine sites (small grey dots) referred to their respective hinterland region. SAH = ODP Site 659; LIB = ODP663; BOS = Lake Bosumtwi; CON = ODP Site 1075; NAM1 = GeoB1028-5; NAM2 = ODP Site1082; LOM = MD96-2048; MAL = Lake Malawi; MAG = Lake Magadi; CHB = Paleolake Chew Bahir; MED = ODP Site 967. Full list of references and coordinates for all sites is provided in Table S1. Blue dots mark marine sites used for the reconstruction of the WC (Table S2); (**B**) Sea surface temperature anomalies and resulting changes in tropical heating and convection (related to WC) under El Niño conditions (positive ENSO phase); (**C**) Sea surface temperature anomalies and resulting changes in tropical heating and convection (related to WC) under La Niña conditions (negative ENSO phase). For more details on the effect of El Niño/La Niña on African precipitation see Supplemenatry Information. Blue area = cooling relative to normal conditions; red areas = warming relative to normal conditions; black arrows indicate transport direction.

Figure 2. Pan-African climate variability during the last ~620 kyr. (**A**) Orbital eccentricity (left) and precession (right) (59); (**B**) Average PC1 loadings derived from the piecewise PCA; (**C**) PC1 derived from the piecewise PCA. *n* = number of data sets used in each iteration; (**D**) comparison between PC1 and the sea-surface temperature gradient (ΔSST; red line) between eastern Pacific Ocean ODP Site 806 (32) and western Pacific Ocean ODP Site 846 (33). Designation of El Niño and La Niña-like conditions follows (30). Break points and their error bounds of PC1 (black boxes), ENSO (red boxes) and Earth´s eccentricity (grey boxes) are marked.

Figure 3. Pan-African climate variability relative to the fossil evidence for hominin evolution during the Middle and Late Pleistocene. (**A**) and (**B**) show the Spearman correlation coefficients for the months October to April from years 1891-2016 of the NINO3.4 index and the Global Precipitation Climatology Centre (GPCC V2018 land) precipitation data in a 0.5° grid. Positive correlation coefficients = humid conditions; negative correlation coefficients = arid conditions. The spatial correlation shown is significant with p>10%. Analysis and visualization: https://climexp.knmi.nl/start.cgi; (**C**) displays the location of the study sites used for the reconstruction of pan-African climate variability. Full list of abbreviations, references, and coordinates for all sites is provided in Table S1; (**D**), (**E**) and (**F**) present the spatiotemporal distribution of moisture during Phases II, III, and IV thus encompassing a full ~400 kyr eccentricity cycle. The designation of humid/arid (blue/red) for each study site (circle) derives from the calculation of the proxy median for the respective time slice relative to the reference median value of the entire data population across the last ~620 kyr (see methods for details; Table S3). List of key hominin fossil sites traces are marked by black triangles (see Table S4 for references). Photos in (D): Ryan Somma/Wikimedia Commons; Photos in (E) from Top: modified from (60); Addis Ababa national museum/Wikimedia Commons.

A

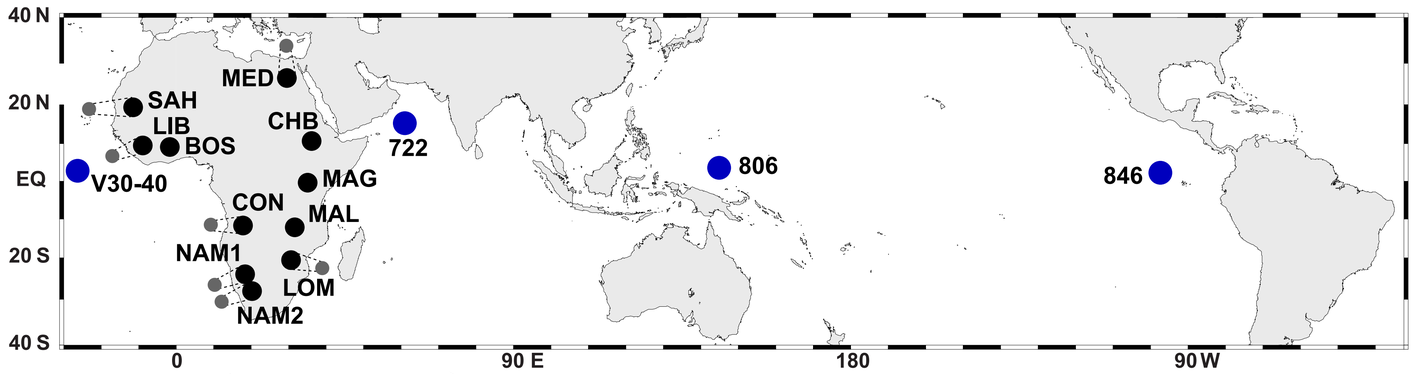
40 N
20 N
EQ
20 S
40 S
0
90 E
180
90 W
MED
SAH
LIB
BOS
CHB
722
806
846
V30-40
MAG
CON
MAL
NAM1
LOM
NAM2

B

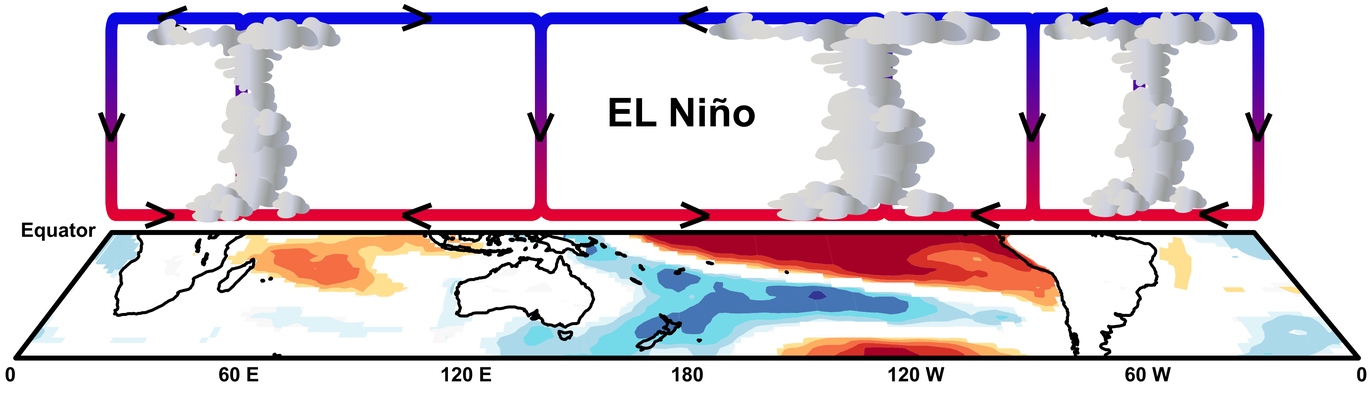
EL Niño
Equator
0
60 E
120 E
180
120 W
60 W
0

C

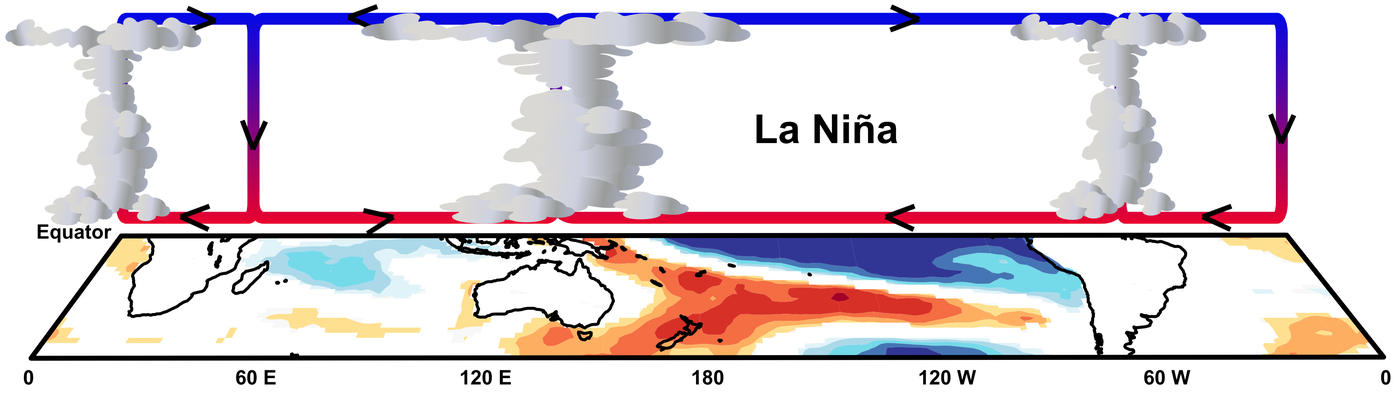
La Niña
Equator
0
60 E
120 E
180
120 W
60 W
0

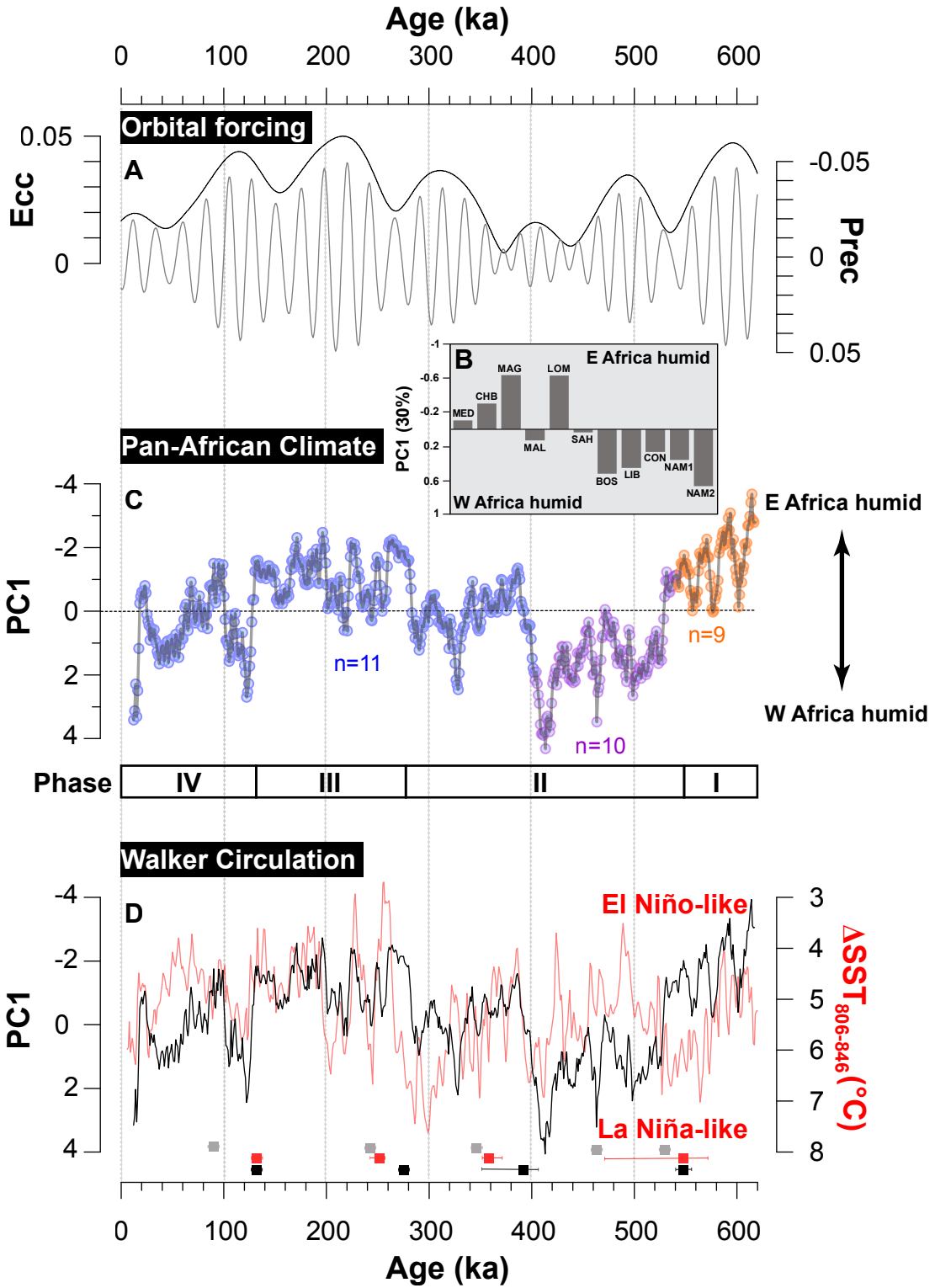
Age (ka)
0
100
200
300
400
500
600
Orbital forcing
A
Ecc
0.05
0
Prec
-0.05
0
0.05
B
E Africa humid
W Africa humid
PC1 (30%)
MED
CHB
MAG
MAL
LOM
SAH
BOS
LIB
CON
NAM1
NAM2
Pan-African Climate
C
PC1
E Africa humid
W Africa humid
n=11
n=10
n=9
Phase
IV
III
II
I
Walker Circulation
D
PC1
El Niño-like
La Niña-like
ΔSST806-846 (°C)
Age (ka)

Modern

Paleoclimate

A

Modern
La Niña conditions

B

Modern
El Niño conditions

humid
0.6
0.5
0.4
0.3
0.2
−0.2
−0.3
−0.4
−0.5
−0.6
arid

C

MED
SAH
LIB
BOS
CHB
MAG
CON
MAL
NAM1
LOM
NAM2

humid
arid
Key Hominin fossils sites

D

Phase II
(525-279 ka)
La Niña-like conditions

E

Phase III
(279-128 ka)
El Niño-like conditions

F

Phase IV
(128-0 ka)
La Niña-like conditions

40 N
20 N
EQ
20 S
40 S
20 W
0
20 E
40 E
60 E

Supplementary Information

Paleo-ENSO influence on African environments and early modern humans

Stefanie Kaboth-Bahr[1,2*], William D. Gosling[3], Ralf Vogelsang[4], André Bahr[2], Eleanor Scerri[5,6], Asfawossen Asrat[7], Andrew S. Cohen[8], Walter Düsing[1], Verena E. Foerster[9], Henry F. Lamb[10,11], Mark A. Maslin[12,13], Helen M. Roberts[10], Frank Schäbitz[9], Martin H. Trauth[1]

[1] University of Potsdam, Institute of Geosciences, Potsdam, Germany

[2] University Heidelberg, Institute of Earth Sciences, Heidelberg, Germany

[3] University of Amsterdam, Institute for Biodiversity and Ecosystem Dynamics, Amsterdam, Netherlands

[4] University of Cologne, Department of Prehistoric Archaeology, Cologne, Germany

[5] Pan-African Evolution Research Group, Max Planck Institute for the Science in Human History, Jena, Germany

[6] Department of Classics and Archaeology, University of Malta, Msida, Malta

[7] Addis Ababa University, School of Earth Sciences, Addis Ababa, Ethiopia

[8] University of Arizona, Department of Geosciences, Tucson, USA

[9] University of Cologne, Institute of Geography Education, Cologne, Germany

[10] Aberystwyth University, Department of Geography and Earth Sciences, Aberystwyth, UK

[11] University of Dublin, Trinity College, Department of Botany, Dublin, Ireland

[12] University College London, Department of Geography, London, UK

[13] Natural History Museum of Denmark, University of Copenhagen, Copenhagen, Denmark

Email: Stefanie Kaboth-Bahr; kabothbahr@uni-potsdam.de

This PDF file includes:

Supplementary Information Text

Site and proxy selection

For the pan-African proxy moisture reconstruction during the Middle and Upper Pleistocene, we selected nine established marine and terrestrial sedimentary archives that meet a number of critical prerequisites: (i) the sites need to be sensitive to moisture changes on the African continent, (ii) sufficient age control must be provided, (iii) the proxy record must at least cover half of the investigated time period of the last ~620 kyr, and (iv) the temporal data resolution should be <5 kyrs to provide sufficient data points for further statistical analysis. We retained the published age model of each individual record as well as their initial proxy record interpretation. The proxy records on their individual age models are shown in Figure S1 as well as site details and proxy explanation are provided in Table S1.

Effect of El Niño/La Niña induced Walker Circulation changes on African precipitation

During El Niño (positive ENSO phase), warming of the eastern and central equatorial Pacific causes ascending motion over the central and eastern Pacific and subsidence over Indonesia (see Fig. 1 in the main text) (1). Over the Indian Ocean this atmospheric configuration leads to a weakening or even reversal of the westerlies initiating pooling of warm water in its northwestern part (positive Indian Ocean Dipole phase). As a consequence, eastern Africa experiences increasingly humid conditions due to the adjacent strong convection over the northwestern Indian Ocean. Increased descending mass fluxes on the western side of the African continent at the same time suppress convection and hence cause aridity over its southern parts (see Fig. 1 in the main text) (1). While El Niño is typically initiated during boreal winter over the Indo-Pacific realm, it incites a lagged response during the subsequent spring-summer over the Atlantic Ocean where intensified trade winds cause the development of a cold tongue of upwelling water along the western African shore (see Fig. 1 in the main text; Atlantic Niño) (2). In combination with the dominant subsidence in western Africa, the reduced evaporation over the cooled eastern equatorial Atlantic increases aridity across southern Africa in boreal winter and in addition the Sahel Zone during boreal summer. In phase with the above discussed alterations of the Walker Circulation (WC), the Hadley Circulation (HC) – which transports moisture latitudinally - also weakens in both hemispheres due to reduced moisture ascension in the African tropics (1). The lack of moisture transport through the HC towards the subtropics adds to the drier conditions under El Niño conditions in south and northwestern Africa in the respective hemisphere summer. During La Niña conditions (negative ENSO phase), the entire system reverses from the El Niño scenario (see Fig. 1 in the main text) leading to the development of a negative Indian Ocean Dipole and Atlantic Niña phase (1). In addition to the outlined mechanism the interferences between WC also causes precipitation anomalies during the subsequent summer months which can vary regionally from the winter counterparts. An example is ENSO interference with the Congo Air Boundary which leads during the summer months also to additional rainfall in western Africa from the Sahel to the Congo basin (1). Although ENSO variability most strongly affects the “short rain” season during the winter months it nevertheless shifts the yearly precipitation budget of these regions to generally wetter or drier conditions relative to non-El Niño years (3, 4). Hence, the temporal changes in precipitation anomalies during the “long rain” season relative to the “short rain” season does not significantly contribute to the overall annual budget change observed during strong ENSO years.

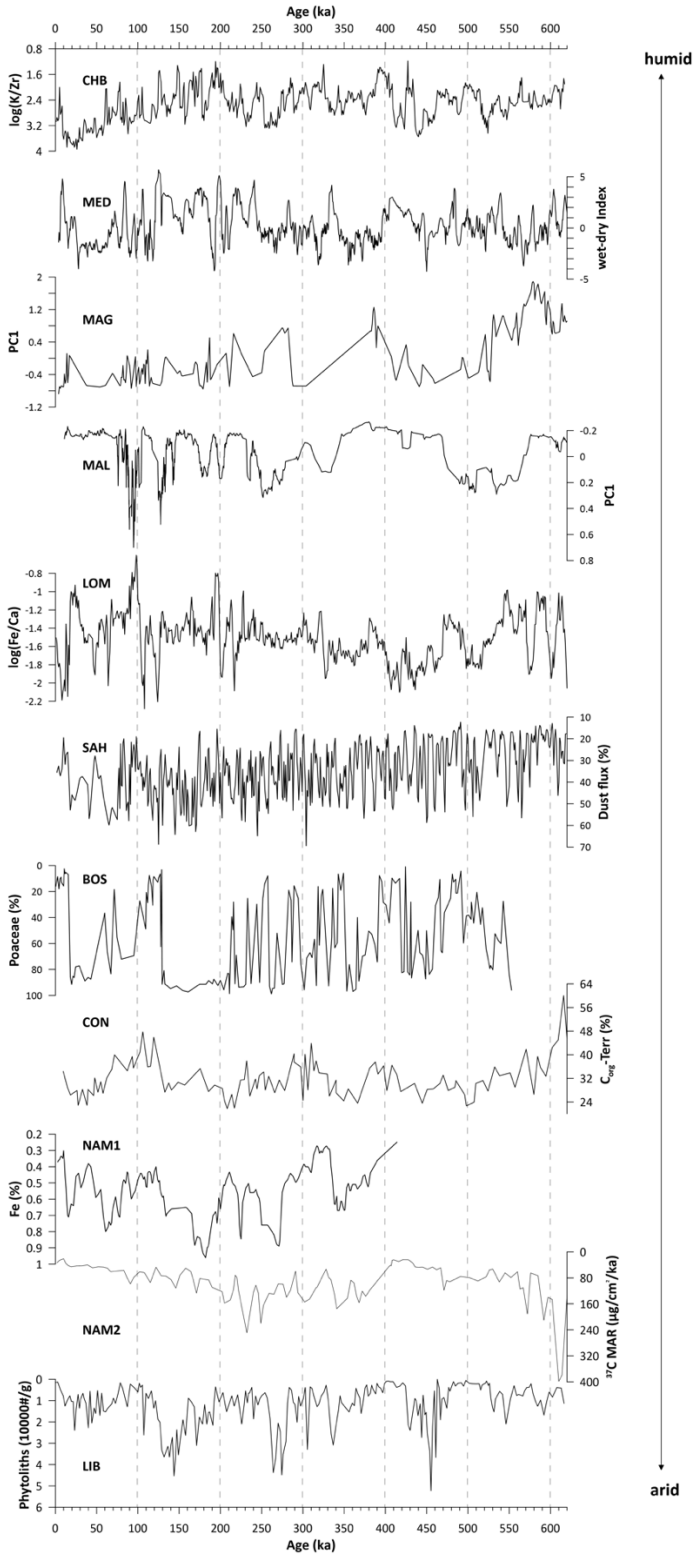

Fig. S1. Overview of the proxy records used for the analysis of pan-African climate change during the last ~620 kyr. All original data sets are presented using their original, published age models. Abbreviations and respective references are listed in Table S1.

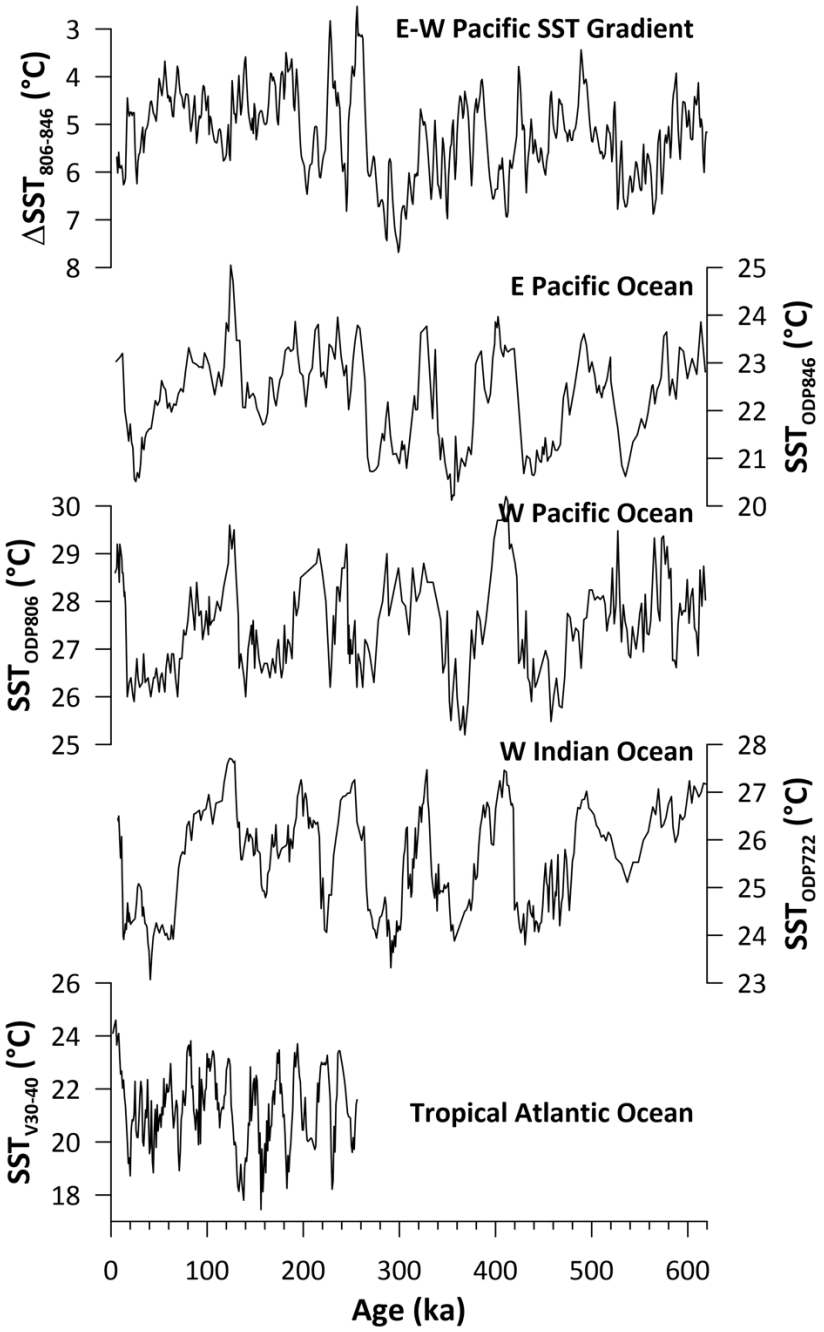

Fig. S2. Overview of the sea-surface temperature (SST) records used for the analysis of El Niño-Southern Oscillation/Walker Circulation changes. All original data sets are presented on their individual age model. Coordinates and respective references are listed in Table S2.

Table S1. Coordinates of African Sites and proxy records used in this study. * denotes marine sediment cores; † denotes terrestrial sediment cores.

Region	Core	Lon (E)	Lat (N)	Age (ka)	Proxy	Proxy interpretation	Reference
MED	ODP967*	29° 39.15'	34° 51.84'	4-620	XRF-based wet-dry index	wet >0 high Nile river run-off; dry <0 low Nile river run-off	(5)
CHB	HSPDP-CHB14-2†	36° 05.00'	4° 01.00'	1-620	log(K/Zr)	wet: high log(K/Zr) values; dry: low log(K/Zr) values	(6)
MAG	HSPDP-MAG14-2A†	36° 16.76'	-01° 51.09'	4-620	Pollen	wet: high PCA1 values of pollen assemblage indicating woodland biome; dry: low PCA1 values of pollen assemblage indicating savannah biome	(7)
MAL	HSDSP-MAL05-1†	34° 24.00'	-11° 12.00'	12-620	PC1	wet: high Lake level; dry low lake level	(8)
LOM	MD96-2048*	34° 01.00'	-26° 10.00'	1-620	log(Fe/Ca)	wet: high terrestrial input via Limpopo river (high Fe/Ca); dry: low terrestrial input via Limpopo river (low Fe/Ca)	(9)
SAH	ODP659*	-21° 01.57'	18° 04.63'	2-620	Dust	Wet: less dust input into the Atlantic Ocean; dry: more dust input into the Atlantic Ocean	(10)
BOS	BOS04-5B†	-1° 02.50'	6° 30.00'	1-552	Poaceae	wet: high Poaceae percentages indicating woodland biome; dry: low Poaceae percentages indicating savannah biome	(11)
CON	ODP1075*	10° 04.98'	-04° 47.11'	9-620	C_{org} -Terr	wet: increased terrigenous organic matter supply by the Congo river to the Congo fan region; dry: decreased terrigenous organic matter supply by the Congo river to the Congo fan region	(12)
NAM 1	GeoB1028-5*	9°11.15'	-20°06.24'	3-413	Fe	wet: low Fe-input through dust plumes into the Atlantic Ocean (Low Fe); dry: high Fe-input through dust plumes into the Atlantic Ocean	(13)
NAM 2	ODP1082*	11° 49.23'	-21° 05.65'	2-620	C^{37} MAR	wet: low off-shore productivity (low C^{37} MAR) due to low coastal upwelling. The warm SST resulting from the lack of cold-water upwelling lead increased humidity transport into the Namib region; dry: high off-shore productivity (high C^{37} MAR) due to high coastal upwelling. The cold SST due to upwelling lead to drought and desertification of Namib region.	(14)
LIB	ODP663*	-11° 52.71'	-1°11.82'	0-620	Phytoliths	Wet: low phytolith concentrations indicate decreased aeolian transport and wetter hinterland conditions; dry: low phytolith concentrations indicate increased aeolian transport and wetter hinterland conditions	(15)

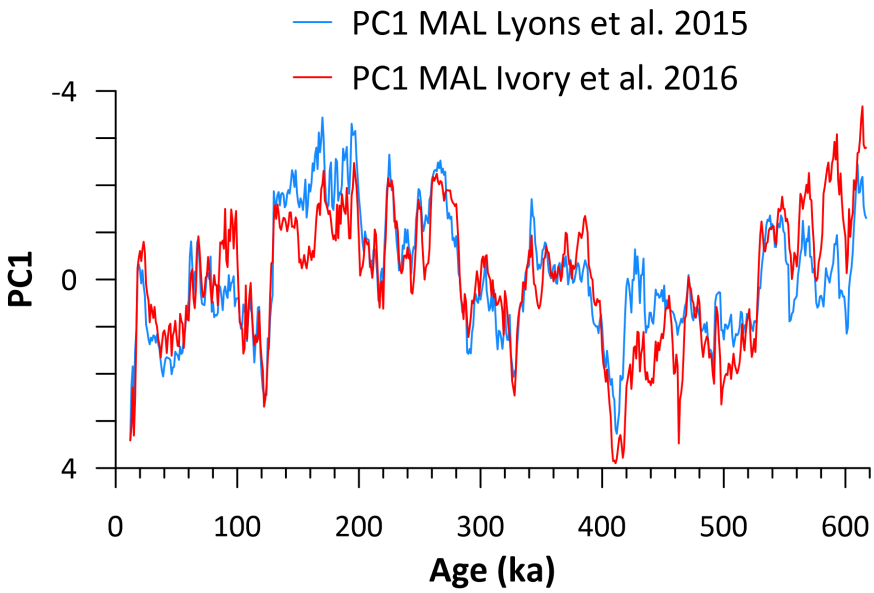

Fig. S3. Comparison of PC1 derived from the piecewise PCA (pwPCA; see methods in main text) of eleven pan-African proxy records using different age models for MAL (see Table S2 for site details). The preferred age model in this study follows (7).

Table S2. Coordinates of sea-surface temperature (SST) records used for the analysis of El Niño-Southern Oscillation/Walker Circulation changes.

Site	Lon (E)	Lat (N)	Reference
ODP 846	-90°49.09'	-3°05.70'	(16)
ODP 806	159°21.66'	0°19.11'	(17)
ODP 722	59°47.71'	16°37.30'	(16)
V30-40	0°12.00'	-23°09.00'	(18)

Table S3. Median calculation of all proxy records used in this study. See Table S1 for site location according to abbreviation. red = arid conditions; blue = humid conditions.

	CHB	MED	MAG	MAL	LOM	SAH	BOS	LIB	CON	NAM1	NAM2
Cut-off	1.09	0.07	-0.04	0.09	-1.49	-1.35	57.75	-1.07	30.29	-0.29	78.96
Phase IV	1.36	-0.91	-0.05	0.15	-1.42	-3.43	20.69	-0.69	30.29	-0.30	46.73
Phase III	1.07	1.12	-0.03	0.03	-1.44	1.72	90.92	-1.81	29.17	-0.21	109.42
Phase II	1.10	-0.10	-0.59	0.09	-1.64	-0.80	49.96	-0.94	32.15	-0.35	78.82

Table S4. Overview of key hominin fossil findings of mid to late Pleistocene age referenced in Figure 3 of the main text.

Location	Age (ka)	References
Bodo D'ar, Ethiopia	600	(19)
Kapthurin Formation, Kenya	509 – 543 (510 - 512)	(20)
Ndutu, Lake Ndutu, Tanzania	490 – 780	(21, 22)
Lainyamok, Kenya	393-300	(23)
Broken Hill, Kabwe 1, Zambia	299 ±25	(24–26)
Cave of Hearth, RSA	200 – 500	(27, 28)
Sidi Abderrahman, La Grottes de Littorine, Morocco	~ 375	(29)
Cameroon	~ 338 (237 – 581)	(30)
Jebel Irhoud, Morocco	315 ± 14	(31, 32)
Dinaledi Chamber, Rising Star Cave System, RSA	236 – 335	(33, 34)
Hoedjiespunt 1, RSA	200 – 300 (125 – 770)	(28, 35)
Florisbad, RSA	224 – 294 (age questioned by Berger & Hawks)	(36–38)
Gawis Cranium, Awash River, Ethiopia	300-500	(39)
Omo Kibish I, II & III, Ethiopia	195 ± 5	(36, 40)
Guomde, East Turkana, Kenya	> 180	(36, 41–43)
Rabat (Kebibat), Morocco	late Middle Pleistocene (125-400)	(36, 44)
Eliye Springs, Kenya	late Middle Pleistocene (125-400)	(36, 45, 46)
El Aliya & Témara, Morocco	Aterian MIS6 (130-190)	(36)
Herto 1 & 2, Ethiopia	154 – 160	(47–50)
Singa, Sudan	131-135	(36, 51–54)
Pinnacle Point 13b, RSA	90 – 100 90 – 162	(55, 56)
Mumba, Tanzania	110 – 130	(57)
Lake Eyasi, Tanzania	88-130	(36, 58, 59)

Grottes de Contrebandiers, Morocco	80-130	(36, 60)
Ysterfontein 1, RSA	71 – 105 50 – 130	(55, 56, 61)
Blind River, RSA	112 – 124	(28, 56)
Ngaloba, Laetoli, Tanzania	120 ± 30	(36, 62–65)
Dar-es-Soltan II 5, Morocco	> 110?	(36, 66, 67)
Klasies River Mouth, RSA	100 ± 25 85 – 110	(21, 36, 56)
Witkrans, RSA	86 – 103 (50 – 100)	(28, 56, 68)
Sea Harvest, RSA	85 – 95 (71 – 110)	(28, 56, 69)
Middle Awash, Bouri & Aduma, Ethiopia	79 - 105	(70)
Equus Cave, RSA	30 – 103	(56, 71)
Plovers Lake, RSA	62.9 – 88.7 62 – 89	(55, 56)
Die Kelders, Cave 1, RSA	59 – 74	(56, 72)
Taramsa Hill, Egypt	50 – 80	(36, 73, 74)
Border Cave, RSA	61 – 72 71 – 91 152 – 171?	(36, 75)
Klipdrift Shelter, RSA	60 – 65 (52 – 72)	(55, 56)
Haua Fteah, Libya	70	(36, 76)
Blombos Cave, RSA	100 - 94 65 – 70 70 – 102	(28, 56, 77)
Sibudu, RSA	64 – 77	(55, 56)
Diepkloof Rock Shelter, RSA	58 – 61	(55, 56)
Ndutu, OH 83, Tanzania	32-60	(78)
Hofmeyer, RSA	36	(79)

SI References

1. C. P. de Oliveira, L. Aímola, T. Ambrizzi, A. C. V. Freitas, The Influence of the Regional Hadley and Walker Circulations on Precipitation Patterns over Africa in El Niño, La Niña, and Neutral Years. *Pure Appl. Geophys*. **175**, 2293–2306 (2018).
2. C. Brierley, I. Wainer, Inter-annual variability in the tropical Atlantic from the Last Glacial Maximum into future climate projections simulated by CMIP5/PMIP3. *Clim. Past* **14**, 1377–1390 (2018).
3. I. Fer, B. Tietjen, F. Jeltsch, C. Wolff, The influence of El Niño-Southern Oscillation regimes on eastern African vegetation and its future implications under the RCP8.5 warming scenario. *Biogeosciences* **14**, 4355–4374 (2017).
4. S. M. Moore, *et al.*, El Niño and the shifting geography of cholera in Africa. *Proc. Natl. Acad. Sci. U. S. A.* **114**, 4436–4441 (2017).
5. K. M. Grant et al., A 3 million year index for North African humidity/aridity and the implication of potential pan-African Humid periods. *Quat. Sci. Rev*. **171**, 100–118 (2017).
6. Trauth et al., Recurring types of variability and transitions in the ~620 kyr record of climate change from the Chew Bahir basin, southern Ethiopia. *Quat. Sci. Rev., in press, doi: 10.1016/j.quascirev.2020.106777*
7. R. B. Owen, *et al*., Progressive aridification in East Africa over the last half million years and implications for human evolution. *Proc. Natl. Acad. Sci. U. S. A.* **115**, 11174–11179 (2018).
8. S. J. Ivory, *et al*., Environmental change explains cichlid adaptive radiation at Lake Malawi over the past 1.2 million years. *Proc. Natl. Acad. Sci. U. S. A*. **113**, 11895–11900 (2016).
9. T. Caley, *et al*., A two-million-year-long hydroclimatic context for hominin evolution in southeastern Africa. *Nature* **560**, 76–79 (2018).
10. R. Tiedemann, M. Sarnthein, N. J. Shackleton, Astronomic timescale for the Pliocene Atlantic $\delta^{18}O$ and dust flux records of Ocean Drilling Program Site 659. *Paleoceanography* **9**, 619–638 (1994).
11. C. S. Miller, W. D. Gosling, D. B. Kemp, A. L. Coe, I. Gilmour, Drivers of ecosystem and climate change in tropical West Africa over the past ~540 000 years. *J. Quat. Sci*. **31**, 671–677 (2016).
12. J. Holtvoeth, T. Wagner, B. Horsfield, C. J. Schubert, U. Wand, Late-quaternary supply of terrigenous organic matter to the Congo deep-sea fan (ODP site 1075): Implications for equatorial African paleoclimate. *Geo-Marine Lett*. **21**, 23–33 (2001).
13. M. Zabel, T. Bickert, L. Dittert, R. R. Haese, Significance of the sedimentary Al:Ti ratio as an indicator for variations in the circulation patterns of the equatorial North Atlantic. *Paleoceanography* **14**, 789–799 (1999).
14. J. Etourneau, P. Martinez, T. Blanz, R. Schneider, Pliocene-Pleistocene variability of upwelling activity, productivity, and nutrient cycling in the Benguela region. *Geology* **37**, 871–874 (2009).
15. P. B. deMenocal, W. F. Ruddiman, E. M. Pokras, Influences of High- and Low-Latitude Processes on African Terrestrial Climate: Pleistocene Eolian Records from Equatorial Atlantic Ocean Drilling Program Site 663. *Paleoceanography* **8**, 209–242 (1993).
16. T. D. Herbert, et al., Late Miocene global cooling and the rise of modern ecosystems. *Nat. Geosci.* **9**, 843–847 (2016).
17. M. Medina-Elizalde, D. W. Lea, The Mid-Pleistocene transition in the tropical Pacific. *Science* **310**, 1009–1012 (2005).
18. A. McIntyre, W. F. Ruddiman, K. Karlin, A. C. Mix, Surface water response of the equatorial Atlantic Ocean to orbital forcing. *Paleoceanography* **4**, 19–55 (1989).
19. G. Bräuer, The origin of modern anatomy: by speciation or intraspecific evolution? *Evol. Anthropol. Issues, News, Rev.* **17**, 22–37 (2008).
20. A. L. Deino, S. McBrearty, $^{40}Ar/^{39}Ar$ dating of the Kapthurin Formation, Baringo, Kenya. *J. Hum. Evol*. **42**, 185–210 (2002).
21. R. G. Klein, The Human Career (University of Chicago Press, 2009).
22. A. R. Millard, A critique of the chronometric evidence for hominid fossils: I. Africa and the Near East 500-50 ka. *J. Hum. Evol*. **54**, 848–874 (2008).
23. R. Potts, A. Deino, Mid-pleistocene change in large mammal faunas of east Africa. *Quat. Res.* **43**, 106–113 (1995).

24. G. P. Rightmire, Patterns of hominid evolution and dispersal in the Middle Pleistocene. *Quat. Int*. **75**, 77–84 (2001).
25. G. P. Rightmire, Middle and later Pleistocene hominins in Africa and Southwest Asia. *Proc. Natl. Acad. Sci. U. S. A*. **106**, 16046–16050 (2009).
26. R. Grün, et al., Dating the skull from Broken Hill, Zambia, and its position in human evolution. *Nature*, 1–4 (2020).
27. O. M. Pearson, F. E. Grine, Re-analysis of the hominid radii from Cave of Hearths and Klasies River Mouth, South Africa. *J. Hum. Evol.* **32**, 577–592 (1997).
28. M. Lombard, C. Schlebusch, H. Soodyall, Bridging disciplines to better elucidate the evolution of early homo sapiens in southern africa. *S. Afr. J. Sci*. **109**, 1–8 (2013).
29. J. P. Raynal, F. Z. Sbihi Alaoui, L. Magoga, A. Mohib, M. Zouak, Casablanca and the earliest occupation of North Atlantic Morocco. *Quaternaire* **13**, 65–77 (2002).
30. F. L. Mendez, et al., An African American paternal lineage adds an extremely ancient root to the human y chromosome phylogenetic tree. *Am. J. Hum. Genet*. **92**, 454–459 (2013).
31. J. J. Hublin, et al., New fossils from Jebel Irhoud, Morocco and the pan-African origin of Homo sapiens. *Nature* **546**, 289–292 (2017).
32. D. Richter, et al., The age of the hominin fossils from Jebel Irhoud, Morocco, and the origins of the Middle Stone Age. *Nature* **546**, 293–296 (2017).
33. L. R. Berger, J. Hawks, P. H. G. M. Dirks, M. Elliott, E. M. Roberts, Homo naledi and Pleistocene hominin evolution in subequatorial Africa. *Elife* **6**, e24234 (2017).
34. P. H. G. M. Dirks, et al., The age of homo naledi and associated sediments in the rising star cave, South Africa. *Elife* **6**, e24231 (2017).
35. D. D. Stynder, J. Moggi-Cecchi, L. R. Berger, J. E. Parkington, Human mandibular incisors from the late Middle Pleistocene locality of Hoedjiespunt 1, South Africa. *J. Hum. Evol*. **41**, 369–383 (2001).
36. C. Stringer, The origin and evolution of homo sapiens. *Philos. Trans. R. Soc. B Biol. Sci*. **371**, 20150237 (2016).
37. R. Grün, et al., Direct dating of Florisbad hominid. *Nature* **382**, 500–501 (1996).
38. L. R. Berger, J. Hawks, Revisiting the age of the Florisbad hominin material. AfricArXiv (2020)
39. J. Quade, J. G. Wynn, The Geology of Early Humans in the Horn of Africa (Geological Society of America, 2008)
40. I. McDougall, F. H. Brown, J. G. Fleagle, Sapropels and the age of hominins Omo I and II, Kibish, Ethiopia. *J. Hum. Evol*. **55**, 409–420 (2008).
41. G. Bräuer, R. Leakey, E. Mbua, A first report on the ER-3884 cranial remains from Ileret/East Turkana, Kenya. Contin. or Replace. *Controv. Homo sapiens Evol*., 111–120 (1992).
42. E. Trinkaus, A note on the KNM-ER 999 hominid femur. *J. Hum. Evol*. **24**, 493–504 (1993).
43. G. Bräuer, Y. Yokoyama, C. Falgueres, E. Mbua, Modern human origins backdated. *Nature* **386**, 337–338 (1997).
44. J.-J. Hublin, "Northwestern African Middle Pleistocene hominids and their bearing on the emergence of Homo sapiens" in Human Roots: Africa and Asia in the Middle Pleistocene, L. Barham, K. Robson-Brown, Eds. (2001), pp. 99–121.
45. G. Bräuer, R. E. Leakey, The ES-11693 cranium from Eliye Springs, West Turkana, Kenya. *J. Hum. Evol.* **15**, 289–312 (1986).
46. G. Bräuer, et al., Virtual Study of the Endocranial Morphology of the Matrix-Filled Cranium from Eliye Springs, Kenya. *Anat. Rec. - Part A Discov. Mol. Cell. Evol. Biol*. **276**, 113–133 (2004).
47. J. D. Clark, et al., Stratigraphic, chronological and behavioural contexts of Pleistocene Homo sapiens from Middle Awash, Ethiopia. *Nature* **423**, 747–752 (2003).
48. T. D. White, et al., Pleistocene Homo sapiens from Middle Awash, Ethiopia. *Nature* **423**, 742–747 (2003).
49. K. Lubsen, R. Corruccini, Morphometric analysis of the Herto cranium (BOU-VP-16/1): Where does it fit? *J. Contemp. Anthropol*. **2**, 1 (2011).
50. R. McCarthy, L. Lucas, A morphometric re-assessment of BOU-VP-16/1 from Herto, Ethiopia. *J. Hum. Evol*. **74**, 11 (2014).
51. A. S. Woodward, A Fossil Skull of an Ancestral Bushman from the Anglo-Egyptian Sudan. *Antiquity* **12**, 190–195 (1938).

52. C. Stringer, L. Cornish, P. Stuart-Macadam, Preparation and further study of the Singa skull from Sudan. *Bull. Br. Museum, Nat. Hist. Geol*. **38**, 347–358 (1985).
53. F. Spoor, C. Stringer, F. Zonneveld, Rare temporal bone pathology of the Singa calvaria from Sudan. *Am. J. Phys. Anthropol*. **107**, 41–50 (1998).
54. F. McDermott, et al., New late-Pleistocene uranium-thorium and ESR dates for the Singa hominid (Sudan). *J. Hum. Evol*. **31**, 507–516 (1996).
55. M. Will, S. El-Zaatari, K. Harvati, N. J. Conard, Human teeth from securely stratified Middle Stone Age contexts at Sibudu, South Africa. *Archaeol. Anthropol. Sci*. **11**, 3491–3501 (2019).
56. F. E. Grine, "The late quaternary Hominins of Africa: The Skeletal evidence from MIS 6-2" in Africa from MIS6-2: Population Dynamics and Paleoenvironments, S. C. Jones, B. Stewart, Eds. (Springer, 2016), pp. 323–381.
57. G. Bräuer, M. J. Mehlman, Hominid molars from a middle stone age level at the Mumba Rock Shelter, Tanzania. *Am. J. Phys. Anthropol*. **75**, 69–76 (1988).
58. G. Bräuer, A. Mabulla, New hominid fossil from Lake Eyasi, Tanzania. *Anthropologie*, 47–53 (1996).
59. M. Domínguez-Rodrigo, et al., A new archaic Homo sapiens fossil from Lake Eyasi, Tanzania. *J. Hum. Evol*. **54**, 899–903 (2008).
60. J. J. Hublin, et al., "Dental Evidence from the Aterian Human Populations of Morocco" in Modern Origins, (Springer, 2012), pp. 189–204.
61. G. Avery, et al., The Ysterfontein 1 Middle Stone Age Rock Shelter and the Evolution of Coastal Foraging. *Goodwin Ser*., 66–89 (2008).
62. M. H. Day, M. D. Leakey, C. Magori, A new hominid fossil skull (L.H. 18) from the Ngaloba Beds, Laetoli, northern Tanzania. *Nature* **284**, 55–56 (1980).
63. M. Grove, et al., Climatic variability, plasticity, and dispersal: A case study from Lake Tana, Ethiopia. *J. Hum. Evol*. **87**, 32–47 (2015).
64. P. Cohen, Fitting a face to Ngaloba. J. Hum. Evol. 30, 373–379 (1996).
65. G. P. Rightmire, Comparison of Middle Pleistocene hominids from Africa and Asia. *Hum. Roots Africa Asia Middle Pleistocene*, 123–133 (2001).
66. K. Harvati, J. J. Hublin, "Morphological Continuity of the Face in the Late Middle and Late Pleistocene Hominins from Northwestern Africa: A 3D Geometric Morphometric Analysis" in Modern Origins, (Springer, 2012), pp. 179–188.
67. R. N. E. Barton, A. Bouzouggar, S. N. Collcutt, J. L. Schwenninger, L. Clark-Balzan, OSL dating of the Aterian levels at Dar es-Soltan I (Rabat, Morocco) and implications for the dispersal of modern Homo sapiens. *Quat. Sci. Rev*. **28**, 1914–1931 (2009).
68. M. L. McCrossin, Human molars from later Pleistocene deposits of Witkrans Cave, Gaap Escarpment, Kalahari Margin. *Glob. Bioeth*. **7**, 1–10 (1994).
69. F. E. Grine, R. G. Klein, Late Pleistocene human remains from the Sea Harvest site, Saldanha Bay, South Africa. S. Afr. J. Sci. 89, 145–146 (1993).
70. Y. Haile-Selassie, B. Asfaw, T. D. White, Hominid Cranial Remains from Upper Pleistocene Deposits at Aduma, Middle Awash, Ethiopia. *Am. J. Phys. Anthropol*. **123**, 1–10 (2004).
71. F. E. Grine, R. G. Klein, Pleistocene and Holocene human remains from Equus cave, South Africa. *Anthropology* **8**, 55–98 (1985).
72. F. E. Grine, Middle Stone Age human fossils from Die Kelders Cave 1, Western Cape Province, South Africa. *J. Hum. Evol*. **38**, 129–145 (2000).
73. P. M. Vermeersch, et al., A middle palaeolithic burial of a modern human at Taramsa hill, Egypt. *Antiquity* **72**, 475–484 (1998).
74. P. Van Peer, P. Vermeersch, E. Paulissen, Chert Quarrying, Lithic Technology, and a Modern Human Burial at the Palaeolithic Site of Taramsa 1, Upper Egypt (Leuven University Press, 2010)
75. R. Grün, P. Beaumont, P. V. Tobias, S. Eggins, On the age of Border Cave 5 human mandible. *J. Hum. Evol*. **45**, 155–167 (2003).
76. K. Douka, et al., The chronostratigraphy of the Haua Fteah cave (Cyrenaica, northeast Libya). *J. Hum. Evol*. **66**, 39–63 (2014).
77. F. E. Grine, C. S. Henshilwood, Additional human remains from Blombos Cave, South Africa: (1999-2000 excavations). *J. Hum. Evol*. **42**, 293–302 (2002).

78. W. B. Reiner, et al., OH 83: A new early modern human fossil cranium from the Ndutu beds of Olduvai Gorge, Tanzania. *Am. J. Phys. Anthropol*. **164**, 533–545 (2017).
79. F. E. Grine, et al., Late pleistocene human skull from Hofmeyr, South Africa, and modern human origins. *Science* **315**, 226–229 (2007).